Axisymmetric stagnation-point flow over a lubricated surface

B. Santra[1], **B. S. Dandapat**[1], **H. I. Andersson**[2]

[1]Physics and Applied Mathematics Unit, Indian Statistical Institute, Calcutta, India
[2]Department of Energy and Process Engineering, The Norwegian University of Science and Technology, Trondheim, Norway

Summary. Axisymmetric stagnation-point flow is considered. A Newtonian fluid impinges orthogonally on a plane surface lubricated by a thin non-Newtonian liquid film of variable thickness. A slip-flow boundary condition is deduced, which allows for partial slip at the surface. The amount of slip, from full slip to no-slip, is controlled by a dimensionless slip coefficient. Similarity solutions are generally prohibited by the slip-flow boundary condition, except for one particular value of the power-law index of the lubricant. Solutions are presented for this case in order to demonstrate the influence of partial slip on the stagnation point flow. With increasing slip and reduced surface stress, a thinning of the viscous boundary layer is observed. The classical Homann flow is recovered in the no-slip limit.

1 Introduction

One of the classical problems in fluid dynamics is the axisymmetric orthogonal stagnation-point flow, first considered by Homann [1] and later by Frössling [2]. Howarth [3] and Davey [4] considered the three-dimensional orthogonal stagnation-point flow of which the axisymmetric case was studied as a special case. Yeckel et al. [5] showed that the classical Homann flow can be used to supply boundary conditions for Reynolds' lubrication equations for flow within a thin viscous film, thereby leading to a model for the thinning of the film in the stagnation region of a turbulent water jet. Wang [6] studied the stagnation-point flow with surface slip that occurs in rarefied flow or under high pressure, while Blyth and Pozrikidis [7] investigated the stagnation-point flow of a Newtonian fluid against a Newtonian liquid film resting on a plane wall. They individually considered several cases for orthogonal two-dimensional, axisymmetric, three-dimensional and oblique two-dimensional flow.

In the present study the steady and axisymmetric stagnation-point flow of a Newtonian bulk fluid impinging orthogonally on a solid surface covered by a non-Newtonian liquid film will be

considered. Such jet-like flows of gases or liquids impinging on a solid surface have several industrial applications which encompass the need to enhance the heat and/or mass transfer. Typical examples are associated with the annealing of metals, cooling of gas turbine blades, cooling in grinding processes [8] and cooling of photovoltaic cells [9]. The shear stress induced by the impinging fluid stream is utilized in surface cleaning [10], paper and photographic film manufacturing, wire coating and finishing of metal strips. In a coating process the thickness of the coating has to be accurately controlled. Excess material is removed by so called doctoring, which can either be mechanical (using scrapers or squeeze rolls), electromagnetic or fluid-mechanical (using, e.g., an air jet to doctor off the excess coating liquid from the substrate). In the present context, conventional no-slip conditions can no longer be applied due to the presence of the lubricating film. A slip-flow boundary condition is therefore first deduced in a similar way as described by Andersson and Rousselet [11]. Some representative similarity solutions for various degree of slip are presented to illustrate the effect of partial slip.

2 Formulation of the flow problem

2.1 Stagnation-point flow equations

Consider a steady axisymmetric stagnation-point flow over a flat disk covered by a thin layer of an inelastic non-Newtonian liquid that obeys the power-law model due to Ostwald and deWaele. The Newtonian bulk fluid first impinges orthogonally on the lubricated surface and thereafter flows radially in all directions along the surface, as depicted in Fig. 1. A cylindrical coordinate system (r, θ, z), where the z-axis is pointing vertically upwards and the origin is at the centre of the disk, is adopted to describe the axisymmetric fluid motion.

The lubricant is introduced at a constant flow rate $Q(m^3/s)$ through a point source opening at the centre O of the infinitely large disk. The centrally introduced lubricant gradually spreads radially outwards and forms a thin lubrication layer of variable thickness $h(r)$. Owing to the mass conservation principle

$$Q = \int_0^{h(r)} U(r,z) 2\pi r dz, \tag{1}$$

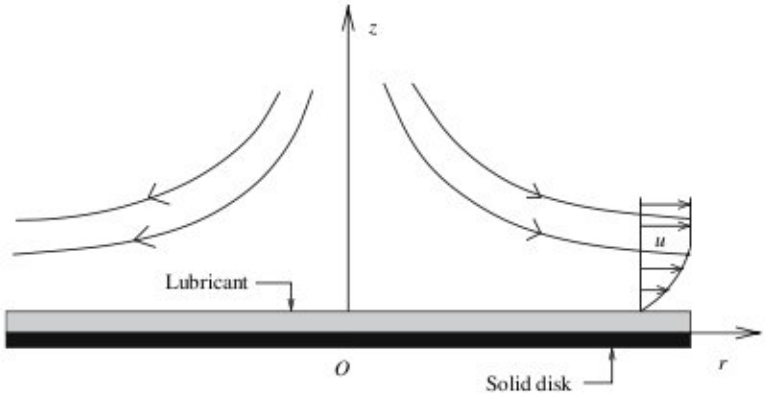

Fig. 1. Schematic of axisymmetric orthogonal stagnation-point flow over a lubricated disk, the z-axis being an axis of symmetry

where $U(r,z)$ represents the radially outward component of the velocity vector $\mathbf{V}=[U,0,W]$ inside the lubricant. The governing equations of the incompressible Newtonian bulk flow $\mathbf{v}=[u,0,w]$ are

$$\frac{\partial u}{\partial r}+\frac{u}{r}+\frac{\partial w}{\partial z}=0, \tag{2}$$

$$u\frac{\partial u}{\partial r}+w\frac{\partial u}{\partial z}=-\frac{1}{\rho}\frac{\partial p}{\partial r}+\nu\left[\frac{\partial^2 u}{\partial r^2}+\frac{\partial}{\partial r}\left(\frac{u}{r}\right)+\frac{\partial^2 u}{\partial z^2}\right], \tag{3}$$

and

$$u\frac{\partial w}{\partial r}+w\frac{\partial w}{\partial z}=-\frac{1}{\rho}\frac{\partial p}{\partial z}+\nu\left[\frac{\partial^2 w}{\partial r^2}+\frac{1}{r}\frac{\partial w}{\partial r}+\frac{\partial^2 w}{\partial z^2}\right], \tag{4}$$

where u and w are the velocities in the radial and axial directions, respectively. p and ν denote the pressure and the kinematic viscosity of the Newtonian bulk fluid, respectively. It is to be noted here that the impinging flow is axisymmetric, i.e. without swirl, implying that the circumferential velocity $v\equiv 0$. Beyond the assumption of steady, axisymmetric flow, no other simplifications have been made. It is particularly noteworthy that the terms representing radial diffusion have been retained. The set of partial differential equations (2)–(4) does therefore not rely on the validity of the boundary layer approximations.

2.2 Boundary conditions

(i) *At the disk* $z=0$:

The impermeability and no-slip conditions at the solid disk give

$$U(r,0)=0, \quad W(r,0)=0. \tag{5}$$

Since there is no axial velocity inside the lubricating film, $W=0$ throughout its depth, i.e.

$$W(r,z)=0 \tag{6}$$

for $z\in[0,h(r)]$.

(ii) *At the interface* $z=h(r)$:

At the interface between the lubricant and the bulk fluid, the velocity and the shear stress components must be continuous. The continuity of the shear stress component at $z=h(r)$ gives

$$\mu\frac{\partial u}{\partial z}=\mu_L\frac{\partial U}{\partial z}, \tag{7}$$

where μ and μ_L denote the viscosity of the Newtonian bulk fluid and the viscosity function of the non-Newtonian power-law type lubricant, respectively. Assuming $\frac{\partial U}{\partial r}\ll\frac{\partial U}{\partial z}$, μ_L here takes the simplified form

$$\mu_L=K\left[\frac{\partial U}{\partial z}\right]^{n-1}, \tag{8}$$

where K and n denote the consistency coefficient and the power-law index of the lubricant, respectively. Following Andersson and Rousselet [11] and Joseph [12] we assume that the radial velocity component U varies linearly from the surface of the disk $z=0$ to the interface between the lubricant and the bulk fluid at $z=h(r)$, i.e.,

$$U(r,z) = \frac{\widetilde{U}(r).z}{h(r)}. \tag{9}$$

Here, $\widetilde{U}(r)$ denotes the interfacial velocity component for both fluids. The local film thickness $h(r)$ can now be expressed as

$$h(r) = \frac{Q}{\pi r \widetilde{U}(r)}. \tag{10}$$

Following the assumption that the lubricant is introduced from a point source at $r = 0$ rather than through a small but finite opening, the expression (10) for the local film thickness becomes singular at $r = 0$. This is of no major concern since the local film thickness $h(r)$ will be eliminated in the subsequent analysis.

Now, using Eqs. (8), (9) and (10) in (7) we get the interfacial condition

$$\frac{\partial u}{\partial z} = \frac{K}{\mu}\left(\frac{\pi}{Q}\right)^n r^n u^{2n}. \tag{11}$$

Continuity of the axial velocity at the interface gives

$$w(r,h(r)) = W(r,h(r)) \tag{12}$$

and the pressure distribution is taken as

$$p(r,h(r)) = -\rho\frac{A^2r^2}{2}, \tag{13}$$

where A is a positive constant indicating the strength of the stagnating flow.

Now Eqs. (6) and (12) together yield

$$w(r,h(r)) = 0. \tag{14}$$

It has already been assumed that the lubrication layer is very thin. Thus, following Joseph [12], the boundary conditions (11), (13) and (14) for the bulk flow can be imposed at the disk $z = 0$ rather than at $z = h(r)$.

(iii) *Far away from the disk*:

Far from the disk, i.e. outside the viscous boundary layer, the bulk flow attains the inviscid free stream solution

$$u = Ar \quad \text{and} \quad w = -2Az \tag{15}$$

in the radial and axial directions, respectively.

2.3 Similarity transformation and resulting ODEs for $n = \frac{1}{3}$

In order to express the system of equations in dimensionless form we choose the similarity transformation

$$z^* = z\sqrt{\frac{A}{\nu}}, \tag{16}$$

$$u = Arf(z^*), \quad w = \sqrt{A\nu}g(z^*), \quad p = A\mu p^*(z^*) - \rho\frac{A^2r^2}{2} \tag{17}$$

and finally obtain the set of non-linear ordinary differential equations (ODEs):

$$g' = -2f, \tag{18}$$

$$f'' = f^2 + gf' - 1, \tag{19}$$

$$p^{*'} = 2fg - 2f', \tag{20}$$

where the prime denotes differentiation with respect to the non-dimensional axial coordinate z^*. In general the similarity transformation (16) and (17) can not remove the explicit appearance of r from the slip-flow boundary condition (11). For the specific value $n = \frac{1}{3}$, however, Eq. (11) transforms exactly to

$$f'(0) = \lambda[f(0)]^{2/3} \tag{21}$$

and thereby assures exact similarity. The above condition (21) along with

$$g(0) = 0 \tag{22}$$

and

$$p^*(0) = 0 \tag{23}$$

are the appropriate boundary conditions for the bulk flow. The outer boundary condition (15) reduces to

$$f \to 1 \text{ as } z^* \to \infty. \tag{24}$$

In Eq. (21), λ represents the dimensionless slip coefficient, given by

$$\lambda = \frac{L_{\text{visc}}}{L_{\text{lub}}} = \frac{\sqrt{v/A}}{(\mu/K)(QA/\pi)^{1/3}}. \tag{25}$$

Here, λ can be interpreted as the ratio between the viscous length scale L_{visc} and the lubrication length L_{lub}. For a small amount of Q of a highly viscous (i.e., large K) lubricant, the lubrication length L_{lub} is small and the slip coefficient λ becomes large. In the limit $\lambda \to \infty$, the conventional no-slip condition $f(0) = 0$ is retrieved from (21). On the contrary, if L_{lub} becomes infinitely large the slip coefficient λ vanishes and full slip $f'(0) = 0$ is achieved. Accordingly, λ can be interpreted as an inverse measure of slip.

Shear-thinning behavior is frequently exhibited by pharmaceutical, chemical and biochemical fluids and processed food. Water gel propellants and various pastes and polymer suspensions behave as power-law fluids with the power-law index n close to 0.3.

3 Numerical solution procedure

The governing ODEs (18)–(20) were expressed as a set of four first-order equations and then integrated numerically by a standard Runge–Kutta technique for different values of the slip coefficient λ in the range from 0.01 to 10. In the computations constant step size $\Delta z^* = 0.001$ was used throughout. The iterative process was terminated when (24) was satisfied to within 10^{-9}. The solution for the no-slip case $\lambda \to \infty$ was obtained with the conventional no-slip boundary condition $f(0) = 0$. Note that if we put $g = -2F$ then Eqs. (18) and (19), respectively, become

$$F' = f \tag{26}$$

and

Table 1. Comparison of the present numerical solution for the no-slip case $\lambda \to \infty$ with that of White [13]

	Present work	White [13]
	$(f'(0) \equiv F''(0) = 1.31193769)$	$(F''(0) = 1.31194)$
	$\Delta z^* = 0.001$	$\Delta z^* = 0.03$
z^*	$f \equiv F'$	F'
0.0	0.0	0.0
0.2	0.24239435	0.24239
0.4	0.44498662	0.44499
0.6	0.60870994	0.60871
0.8	0.73577289	0.73577
1.0	0.82986805	0.82987
1.2	0.89597727	0.89598
1.4	0.93982673	0.93983
1.6	0.96717382	0.96718
1.8	0.98315816	0.98316
2.0	0.99189216	0.99190
2.2	0.99634476	0.99635
2.4	0.99845935	0.99847
2.6	0.99939375	0.99940
2.8	0.99977755	0.99979
3.0	0.99992397	0.99993

$$F''' + 2FF'' + 1 - F'^2 = 0. \tag{27}$$

Equation (27) together with $F = F' = 0$ and $F' \to 1$ as $z^* \to \infty$ represents the classical axisymmetric stagnation-point, viz. Homann flow [1]. Relation (26) enables verification of the accuracy of the numerical integration for the no-slip case. Table 1 provides a comparison between the present results for the Homann flow and those tabulated in [13]. It is readily observed that the two data sets compare to within 0.00001. The minor discrepancies are probably due to different termination criteria for the iterative solution process and different step sizes.

4 Results and discussions

First, profiles of the radial and wall-normal velocity components and the pressure are presented for some characteristic values of the slip coefficient λ in the range from 0.05 to 2 in Figs. 2–4, together with the corresponding profiles for the no-slip case $\lambda \to \infty$. The radial velocity profiles f in Fig. 2 show that the outward velocity of the bulk fluid along the lubricated surface increases with increasing slip, i.e., as the slip coefficient λ is reduced. As the slip velocity $f(0)$ increases, the amount of adaption of the velocity from the lubricated surface to its free stream value $f = 1$ is reduced. It is intuitively clear that the flow field in the viscous boundary layer approaches the potential solution (15) in the limiting case as λ tends to zero (i.e., full slip). In terms of the similarity variables, the free stream solution yields $f = 1$ and $-g = 2z^*$. This is also a solution of the ODEs (18) and (19) subjected to the boundary conditions $f(0) = 1$ and $g(0) = 0$.

Obeying the mass conservation equation (18) the radial outward flow f is balanced by an axial inward flow $-g$ towards the surface, as shown in Fig. 3. The enhancement of this axial

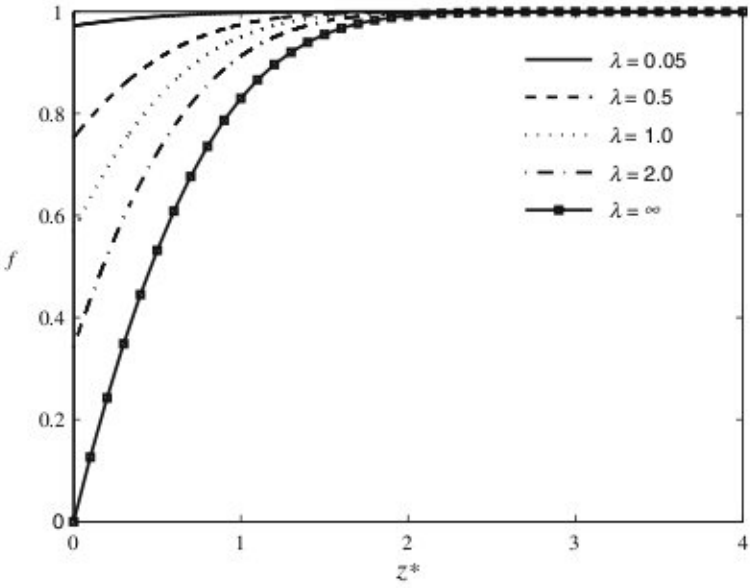

Fig. 2. Similarity radial velocity profiles $f(z^*)$ for various values of the slip coefficient λ

inflow, as observed for the lower λ-values, is therefore a natural consequence of the increased radial outflow for higher slip. It is readily seen that the axial inflow approaches the linear full-slip solution $-g = 2z^*$ for the lowest λ-value shown.

The variation of the pressure profiles $-p^*$ with z^* is presented in Fig. 4. As in the classical Homann-flow (i.e., the no-slip case), the pressure increases towards the surface in the stagnation zone and $-p^*$ exhibits a minimum at $z^* = 0$. The pressure variation across the boundary layer seems to increase with increasing slip, and the most pronounced pressure build-up is found for full-slip. This observation may as first sight appear as a paradox. Let us therefore

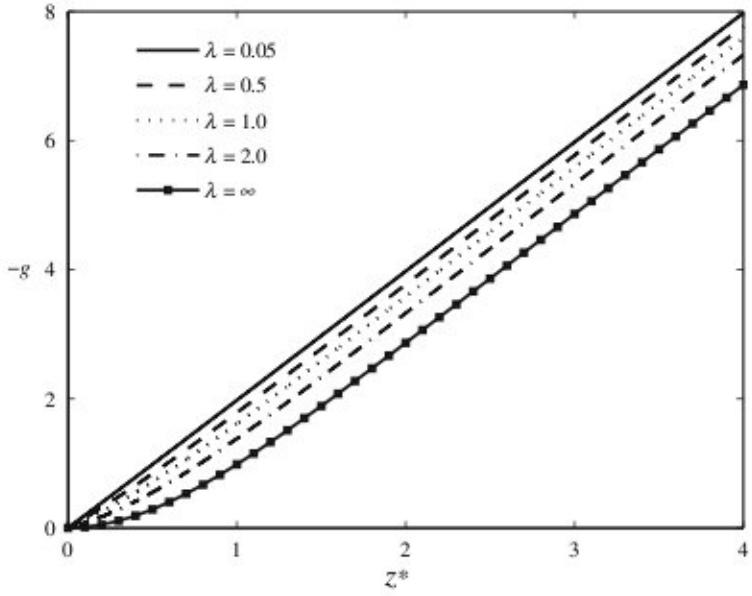

Fig. 3. Similarity axial velocity profiles $-g(z^*)$ for various values of the slip coefficient λ

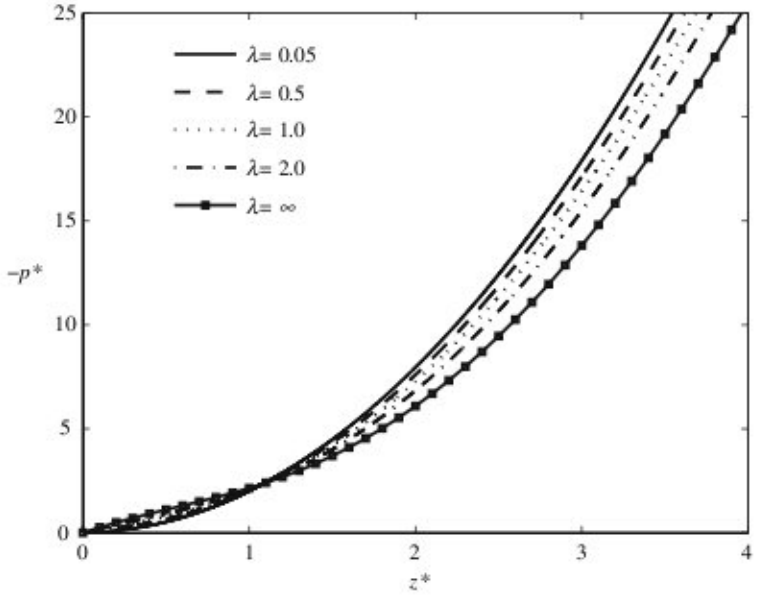

Fig. 4. Similarity pressure profiles $-p^*(z^*)$ for various values of the slip coefficient λ

look at the axial momentum equation (20). By first replacing f and f' by $0.5g'$ and $0.5g''$, respectively, and thereafter integrating once, we find

$$-p^* = 0.5g^2(z^*) + 2(f(z^*) - f(0)). \tag{28}$$

In the full slip case $g = -2z^*$ and $f = 1$ and Eq. (28) simplifies to the parabolic relation $-p^* = 0.5g^2 = 2z^{*2}$. For the high-slip case $\lambda = 0.05$ in Fig. 4, the pressure variation closely resembles the full-slip parabola.

It is evident from Fig. 4 that the pressure curves intersect slightly beyond $z^* = 1$. A closer inspection of the profiles reveals that the crossings of the profiles do not occur in one single point. According to Eq. (28), the pressure is affected both by the radial and the axial velocity components, which in turn are affected differently by interfacial slip. Figure 3 shows that $0.5g^2(z^*)$ increases with increasing slip, whereas Fig. 2 shows that $(f(z^*) - f(0))$ decreases with increasing slip. The latter effect is dominating in the immediate vicinity of the surface and thereby explains why $-p^*$ is reduced below its no-slip level close to the surface.

The pressure distribution in the classical Homann flow exhibits an inflection point somewhat above the surface and this inflection point seems to shift towards the surface with increasing amount of slip. Let us thus differentiate the axial momentum equation (20) and thereafter eliminate g and g'. Then, by equating p'' to zero, we find that an inflection point in the pressure distribution coincides with the axial position at which $f = 1/\sqrt{3} \approx 0.577$. Since the radial velocity component f is a monotonically increasing function of z^*, the inflection point vanishes as soon as the slip velocity $f(0)$ exceeds $1/\sqrt{3}$. With the aid of the velocity profiles in Fig. 2, we can therefore conclude that the pressure distribution exhibits an inflection point only as long the slip coefficient λ is above unity.

Figure 5 summarizes the effect of slip on the radial slip velocity $f(0)$, the surface shear stress $f'(0)$ and on the displacement thickness δ^* deduced from the formula

$$\delta^* = 0.5 \lim_{z^* \to \infty} [2z^* + g(z^*)]. \tag{29}$$

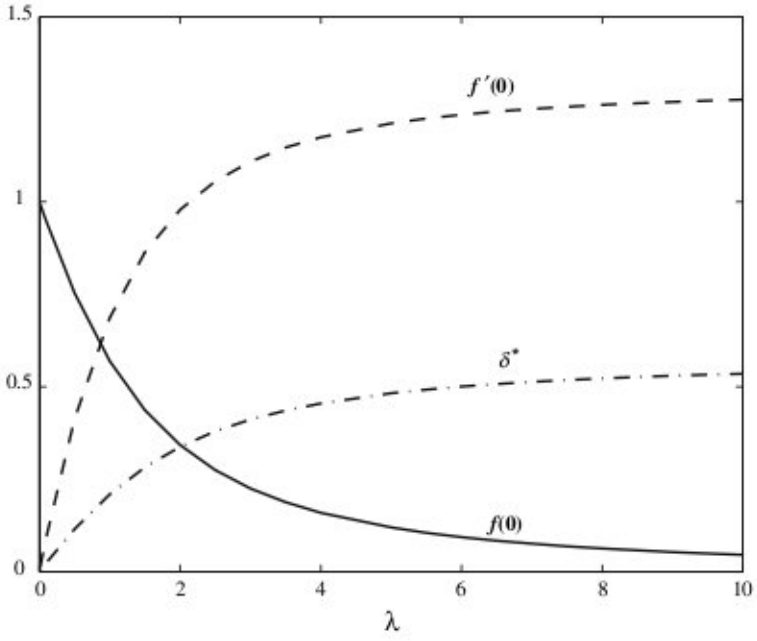

Fig. 5. Effect of the slip coefficient λ on some flow characteristics: Slip velocity $f(0)$, surface shear stress $f'(0)$ and displacement thickness δ^*

The radial slip velocity $f(0)$ approaches asymptotically towards 0 as λ becomes large, while the surface shear stress $f'(0)$ increases monotonically from 0 (corresponding to the full-slip case $\lambda = 0$) to its limiting value 1.312 in the no-slip case. The variation of the displacement thickness δ^* with λ demonstrates the thinning of the momentum boundary layer in the bulk fluid with increasing amount of interfacial slip. Since the displacement thickness is a measure of the outward shift of the external streamlines due the presence of the viscous boundary layer, it is not surprising to find the largest displacement thickness 0.5689 in the no-slip limit as λ tends to infinity.

Let us finally recall that although the interfacial slip-flow condition (11) is valid for any positive value of the power-law index n, the governing equations for the axisymmetric stagnation-point flow in Sect. 2.1 transform into ordinary differential equations only for $n = 1/3$, i.e., for a particular shear-thinning lubricant. For any other value of the power-law index n, the slip-flow condition (11) prohibits exact similarity to be achieved. This does only imply that one has to resort to the partial differential equations in Sect. 2.1 rather than the ordinary differential equations in Sect. 2.3. It is believed that the general influence of partial slip, as observed herein for the particular parameter value $n = 1/3$, will be seen also for other values of the power-law index, including also Newtonian lubricants $n = 1$.

5 Conclusions

Axisymmetric stagnation-point flow of a Newtonian fluid has been examined. In order to allow for partial slip, the surface on which the flow stagnates was lubricated by a thin liquid film of a power-law fluid. For the particular value of the power-law index $n = 1/3$, the governing equations of motion transform to ODEs by means of a similarity transformation. The resulting slip condition $f'(0) = \lambda(f(0))^{2/3}$ can be regarded as a generalized boundary condition for the

stagnating flow, such that $\lambda = 0$ implies full slip and $\lambda \to \infty$ represents the conventional no-slip condition. The computed results showed that the effect of slip is to increase the radial outflow and reduce the accompanying surface shear stress. As the thickness of the viscous boundary layer is reduced with increasing slip, the pressure build-up in the stagnation zone turned out to increase. The solution of the classical Homann flow is recovered in the limit $\lambda \to \infty$.

Acknowledgements

The first author (B.S.) is grateful to The University Grants Commission, New Delhi, India, for providing Teacher Fellowship (vide memo no. F.TF.W4 - 002 - 02/06 - 07(ERO)) and the College Authority of Jangipur College, Murshidabad, W.B., India, for granting the leave during the period of work.

References

[1] Homann, F.: Der Einfluss grosser Zähigkeit bei der Strömung um den Zylinder und um die Kugel. Z. angew. Math. Mech. (ZAMM) **16**, 153–164 (1936).
[2] Frössling, N.: Verdunstung, Wärmeübertragung und Geschwindigkeitsverteilung bei zweidimensionaler und rotationssymmetrischer laminarer Grenzschichtströmung. Lunds Univ. Arsskr. N.F. Avd. 2, **35**, No. 4 (1940).
[3] Howarth, L.: The boundary layer in three-dimensional flow. Part II: The flow near a stagnation point. Phil. Mag. VII **42**, 1433–1440 (1951).
[4] Davey, A.: Boundary layer flow at a saddle point of attachment. J. Fluid Mech. **10**, 593–610 (1961).
[5] Yeckel, A., Strong, L., Middleman, S.: Viscous film flow in the stagnation region of the jet impinging on planar surface. AIChE J. **40**, 1611–1617 (1994).
[6] Wang, C. Y.: Stagnation flows with slip: exact solutions of the Navier–Stokes equations. Z. Angew. Math. Phys. (ZAMP) **54**, 184–189 (2003).
[7] Blyth, M. G., Pozrikidis, C.: Stagnation-point flow against a liquid film on a plane wall. Acta Mech. **180**, 203–219 (2005).
[8] Babic, D., Murray, D. B., Torrance, A. A.: Mist jet cooling of grinding process. Int. J. Mach. Tools Manufact. **45**, 1171–1177 (2005).
[9] Royane, A., Dey, C.: Experimental study of a jet impingement device for cooling of photovoltaic cells under high concentration. Proc. Solar 2004: Life, the Universe and Renewables (2004).
[10] Phares, D. J., Smedley, G. T., Flagan, R. C.: The inviscid impingement of a jet with arbitrary velocity profile. Phys. Fluids **12**, 2046–2055 (2000).
[11] Andersson, H. I., Rousselet, M.: Slip flow over a lubricated rotating disk. Int. J. Heat Fluid Flow **27**, 329–335 (2006).
[12] Joseph, D. D.: Boundary conditions for thin lubrication layers. Phys. Fluids **23**, 2356–2358 (1980).
[13] White, F. M.: Viscous fluid flow, 2nd ed., p. 156. Mc-Graw Hill 1991.